JACS
JOURNAL OF THE AMERICAN CHEMICAL SOCIETY
pubs.acs.org/JACS
Article

Photoinduced Charge Transfer with a Small Driving Force Facilitated by Exciplex-like Complex Formation in Metal–Organic Frameworks

Xinlin Li, Jierui Yu, Zhiyong Lu, Jiaxin Duan, H. Christopher Fry, David J. Gosztola, Karan Maindan, Sreehari Surendran Rajasree, and Pravas Deria*

Cite This: J. Am. Chem. Soc. 2021, 143, 15286–15297
Read Online

ABSTRACT: Photoinduced charge transfer (PCT) is a key step in the light-harvesting (LH) process producing the redox equivalents for energy conversion. However, like traditional macromolecular donor–acceptor assemblies, most MOF-derived LH systems are designed with a large ΔG^0 to drive PCT. To emulate the functionality of the reaction center of the natural LH complex that drives PCT within a pair of identical chromophores producing charge carriers with maximum potentials, we prepared two electronically diverse carboxy-terminated zinc porphyrins, BFBP(Zn)-COOH and TFP(Zn)-COOH, and installed them into the hexagonal pores of NU-1000 via solvent-assisted ligand incorporation (SALI), resulting in BFBP(Zn)@NU-1000 and TFP(Zn)@NU-1000 compositions. Varying the number of trifluoromethyl groups at the porphyrin core, we tuned the ground-state redox potentials of the porphyrins within ca. 0.1 V relative to that of NU-1000, defining a small ΔG_0 for PCT. For BFBP(Zn)@NU-1000, the relative ground- and excited-state redox potentials of the components facilitate an energy transfer (EnT) from NU-1000* to BFBP(Zn), forming BFBP$(Zn)_{S1}$* which entails a long-lived charge-separated complex formed through an exciplex-like [BFBP$(Zn)_{S1}$*–TBAPy] intermediate. Various time-resolved spectroscopic data suggest that EnT from NU-1000* may not involve a fast Förster-like resonance energy transfer (FRET) but rather through a slow [NU-1000*–BFBP(Zn)] intermediate formation. In contrast, TFP(Zn)@NU-1000 displays an efficient EnT from NU-1000* to [TFP(Zn)–TBAPy], a complex that formed at the ground state through electronic interaction, and thereon showed the excited-state feature of [TFP(Zn)–TBAPy]*. The results will help to develop synthetic LHC systems that can produce long-lived photogenerated charge carriers with high potentials, i.e., high open-circuit voltage in photoelectrochemical setups.

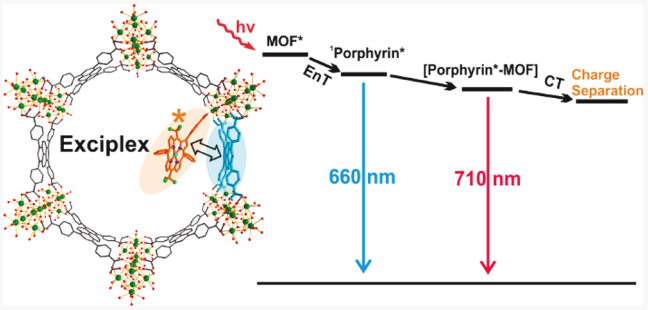

INTRODUCTION

Efficient solar energy conversion in natural photosynthetic apparatus is achieved by the elegant organization of photosynthetic pigments within the protein framework of the light-harvesting complex (LHC). While the special chromophore pair reaction center (RC), at the middle of the LHC, absorbs the photon energy and prepares the redox equivalents (charge carriers with sufficiently high potentials) to drive NAD(P)H formation for CO_2 reduction in PS-I and water oxidation in PS-II, the arrays of chlorophylls and carotenes are responsible for capturing the sunlight and transferring energy to activate the RC. The working principle in the LHC has inspired the development of efficient artificial energy conversion systems.[1−3] Among various factors, the key requirements for an artificial LH system are its panchromatic sensitization encompassing a large region of the visible spectrum, efficient delivery of the excitonic energy to the reaction center to produce redox equivalents, and a long charge recombination time to drive the desired redox transformations.[4,5] However, assembling solid compositions featuring these functionalities, without being infested by various wasteful exciton recombination pathways, has been challenging.[6−10]

Crystalline metal–organic frameworks (MOFs), constructed from a wide range of photo- and redox-active metal nodes and organic struts, offer a unique platform for developing such artificial LHCs.[11−15] Precise relative positioning of these functional building blocks offer predictable interchromophoric interactions that are critical for energy transfer (EnT) and photoinduced charge transfer (PCT) processes. The topology-controlled structural variation and other modularity bring up the most important feature: scalable tunability of photophysical processes.[16−18] Furthermore, tailored functionalities, achieved

Received: June 25, 2021
Published: September 9, 2021

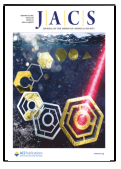

https://doi.org/10.1021/jacs.1c06629
J. Am. Chem. Soc. 2021, 143, 15286–15297

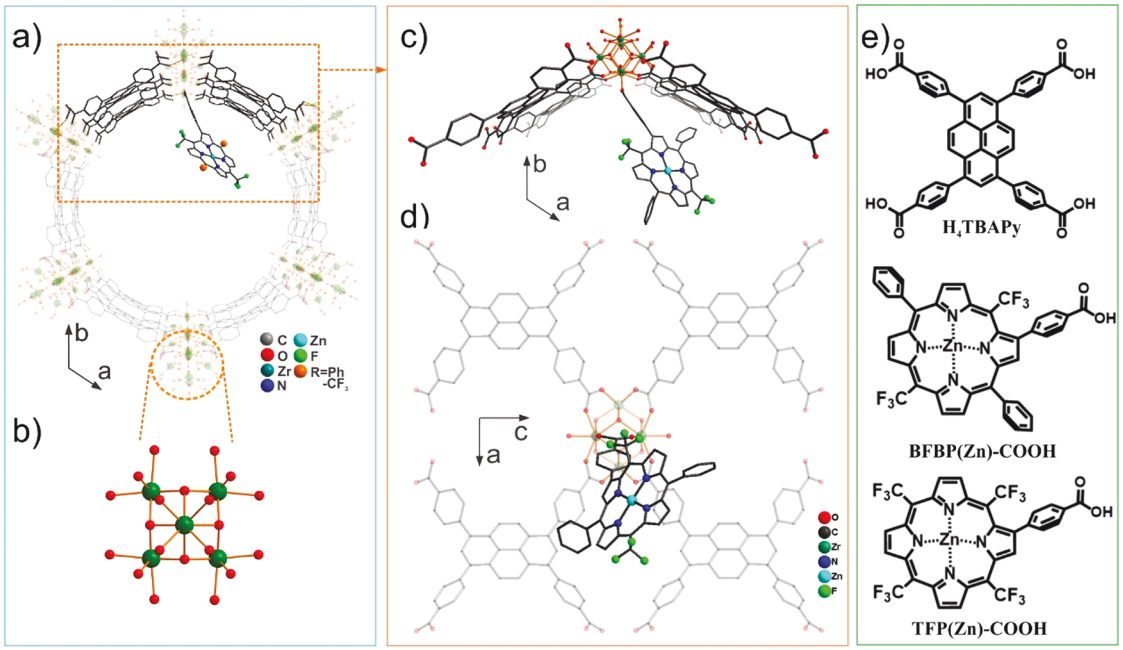

Figure 1. (a, b) Representative structure and components of porphyrin@NU-1000 highlighting the node-installed porphyrin at the hexagonal mesopore of NU-1000. (c, d) Computationally optimized model of BFBP(Zn)@NU-1000 (along the *c* and *b* axis) showing the position of the porphyrin relative to the adjacent TBAPy linkers. (e) Chemical structure of H_4TBAPy, BFBP(Zn)-COOH, and TFP(Zn)-COOH.

through various postsynthesis approaches such as linker exchange and solvent-assisted ligand incorporation (SALI), are always attractive in developing functional systems.[19−22] Indeed, postsynthesis installation of complementary photo- and redox-active species within the MOFs pores has been established for EnT or PCT processes.[23−28]

While macromolecular and supramolecular compositions consisting of donor−acceptor (D-A) motifs have been generally exploited as promising LH components,[29−32] systematic development to underpin the working principle and improve the fundamental EnT and/or PCT processes in MOF-derived systems are rare. We have established that MOF excited states are delocalized where the molecular excitons span multiple linkers.[33] With a node-installed redox quencher in the 1D mesopores of TBAPy-based (TBAPy = 1,3,6,8-tetrakis(*p*-benzoic acid)pyrene) zirconium-MOF NU-1000, we have demonstrated the antenna effect where multilinker excitons are efficiently displaced (requiring a lower number of hops) to redox sites before getting involved in the fast PCT (τ_{CT} ∼ 10 ps) process.[22,33,34] On the basis of these unique findings, we have developed an artificial antenna system in NU-1000 by anchoring a carboxyphenyl-appended tetraphenylporphyrinato zinc(II) (TPP(Zn)-COOH) onto Zr_6-oxo secondary building units (SBUs) via SALI.[35] With complementary pigments, based-on their relative ground-state and excited-state redox potentials, installed within MOF pores, this TPP(Zn)@NU-1000 was established to emulate the antenna functionality of the chlorophyll-based LHCs. The initial photogenerated excitons (NU-1000*) are efficiently transported to the TPP(Zn) site with $k_{EnT} \approx 4.7 \times 10^{11}$ s^{-1} and a PCT resulting in a charge-separated complex [$TBAPy^{\bullet-}$−$TPP(Zn)^{\bullet+}$] with $k_{CT} = 1.2 \times 10^{10}$ s^{-1}.[35] This artificial porous LHC allows a panchromatic excitation (350−600 nm) leading to [$TBAPy^{\bullet-}$−$TPP(Zn)^{\bullet+}$] formation.

While TPP(Zn)@NU-1000 entailed many key targeted features of porous artificial LH systems, especially a fast EnT and efficient PCT, it could produce redox equivalents that are not characterized by their maximum possible potentials. With a sizable ΔG^0 driving the PCT (stemming from the energy difference between $E_{ox}^{TPP(Zn)*}$ and $E_{red}^{NU\text{-}1000}$ of ∼0.46 V), the hybrid could generate redox equivalents with a maximum possible potential difference of ∼1.6 eV (i.e., the open-circuit voltage, V_{OC}, measured from the gap between E_{red}^{A} and E_{ox}^{D}), which is significantly lower than its maximum possibility of ca. 2.1 eV. Like the RC of natural LHC, redox equivalents with maximum potentials can be achieved by closely positioning a pair of quadrupolar aromatic chromophores in a homogeneous solution or crystalline film configuration.[36−41]

While single linker-based MOFs are common, a symmetry-breaking PCT within the pair of the same species has not been achieved. Instead, we investigate here a PCT within the pair of two different chromophores with low ΔG^0, through manipulation of relative energetics of D-A species. For that, we build on the porphyrin@NU-1000 system (Figure 1) where we use two separate porphyrin derivatives possessing electrochemical and optical bandgaps that are comparable to the electrochemical potentials and bandgap of the host NU-1000 antenna to study PCT involving porphyrin* and the MOF. Two carboxy-terminated zinc porphyrins, [2-((4′-carboxy)phenyl)-5,15-bis(trifluoromethyl)-10,20-bis(phenyl)porphyrinato]zinc-(II) (BFBP(Zn)-COOH) and [2-((4′-carboxy)phenyl)-5,10,15,20-tetrakis(trifluoromethyl)porphyrinato]zinc(II) (TFP(Zn)-COOH), were prepared and installed into the hexagonal pores of NU-1000 via SALI (Figures 1a and 3d), resulting in BFBP(Zn)@NU-1000 and TFP(Zn)@NU-1000 compositions. The electronic properties of the porphyrins were modified by replacing the meso-substituted phenylenes with trifluoromethyl (CF_3) groups such that the electrochemical redox potentials of BFBP(Zn) and TFP(Zn) are within ca. ±0.1 V (entailing essentially the same bandgap of ∼2 eV). On the basis of the ground-state and excited-state redox potentials of the respective components and the prepared hybrids, both

https://doi.org/10.1021/jacs.1c06629
J. Am. Chem. Soc. 2021, 143, 15286−15297

were expected to drive PCT with a small driving force. Probed with various steady-state and time-resolved spectroscopies, BFBP(Zn)@NU-1000 showed a fast formation of a low-energy emissive exciplex-like [BFBP(Zn)$_{S1}$*−TBAPy] intermediate, which relaxes to a CT state that partially recombines to ground state and partly decays to a triplet manifold. In contrast, TFP(Zn)@NU-1000 formed a ground-state complex through electronic interaction due to a short TFP(Zn)−TBAPy distance achieved via a nonplanar porphyrin core and displayed excited-state features and dynamics characteristics of this complex; i.e., no dissociative exciplex-like state was observed in TFP(Zn)@NU-1000. We believe that this fundamental study on exciton splitting through an excited-state complex formation in MOFs will shine new light on the development of MOF-based artificial LHC to generate high potential charge carriers.

MATERIALS AND METHODS

Materials and Synthesis. Anhydrous 2-methyltetrahydrofuran (MeTHF) and α,α,α-trifluorotoluene (CF_3Tol) solvents, used for spectroscopic studies, were purchased from Fisher Scientific. Solvents used for synthesis are described in Supporting Information (SI). Phase-pure NU-1000 was synthesized and activated according to a reported procedure.[42,43] Synthesis of carboxy-appended zinc-porphyrins in their respective ester form, BFBP(Zn)-COOEt and TFP(Zn)-COOEt, and their subsequent hydrolysis resulting in the titled compounds BFBP(Zn)-COOH and TFP(Zn)-COOH are described in SI. Porphyrin@NU-1000 samples are prepared via a well-established SALI process also described in SI.[35]

Instrumentation. Cyclic voltammograms (CV) for homogeneous and solid-state samples were recorded on an Autolab 128N potentiostat using a standard three-electrode cell equipped with a platinum counter electrode, an Ag/AgCl (3 M KCl) reference electrode, and a working electrode. The preparation of working electrodes for different samples is detailed in SI. Thermogravimetric analysis (TGA) was carried out on a TGA Q50. Scanning electron microscopy (SEM) and energy-dispersive spectroscopy (EDS) were performed on a Quanta FEG 450 scanning electron microscope. Excitation−emission spectra and absolute quantum yields (QY) were collected on an Edinburgh FS5 spectrofluorimeter. Time-resolved emission spectra (TRES) were collected on an Edinburgh Lifespec II picosecond time-correlated single-photon counting (TCSPC) spectrophotometer. Femtosecond transient absorption spectroscopic data were collected on an HELIOS Ultrafast Systems. Global target fitting was performed using the Glotaran package.[44] Instrumental details along with experimental conditions are described in SI.

RESULTS AND DISCUSSION

Synthesis and Characterization. The carboxy ester-terminated porphyrins, BFBP(Zn)-COOEt and TFP(Zn)-COOEt, were synthesized through Suzuki coupling reactions of the corresponding monobrominated porphyrins. The ester products were then separately hydrolyzed with aqueous potassium hydroxide and carefully acidified to pH 3 with dilute hydrochloric acid (1 M HCl) to afford the carboxyphenyl-terminated zinc porphyrins, BFBP(Zn)-COOH and TFP(Zn)-COOH. Besides ^{1}H NMR data, the zinc(II)-metalated porphyrins were characterized by their two Q bands signature in UV−Vis spectra between 525 and 650 nm (Figure S16) and fluorescence peaks appearing at ca. 620 and 650 nm (Figure S17). Before the porphyrin installation, phase-pure NU-1000 was solvothermally activated by reacting with HCl in dimethyl sulfoxide (DMSO) at 100 °C to liberate the node-bound biphenyl-4-carboxylic acid that was used as the crystal-growth modulator (Figures 1a and 3d). Recent work by Hupp and co-workers have shown the use of DMSO solvent during this activation process leading to a protonated, 8-connected node (with Cl^- as counterion; Figure S7) compared to Zr_6 nodes being blocked by formate-capping achieved via traditional activation performed in *N*,*N*-dimethylformamide (DMF).[45] Formate-free NU-1000 was used as the suitable SALI precursor.[43] The SALI reaction was carried out at 80 °C with 1:1 molar ratio between porphyrin derivatives and Zr-SBUs (i.e., one porphyrin per node target loading). The porphyrin-installed samples displayed less solvent-accessible pores in TGA profiles compared to unmodified NU-1000 precursors (Figure S6). The UV−Vis spectra of the corresponding base-digested compositions (Figure S9) revealed that the porphyrin loading in BFBP(Zn)@NU-1000 and TFP(Zn)@NU-1000 is about one per two nodes (0.59 and 0.49 porphyrin moieties per SBU, respectively); this loading amount is consistent with the SEM-EDS results (Figures S4 and S5). The nonplanarity of the porphyrin ring and the overall steric hindrance that it conveys to the anchoring benzoate at the Zr-node binding site led to a kinetically challenged loading. This geometric limitation in SALI installation (which inherently involves acid−base equilibrium chemistry) will, therefore, ensure evenly distributed porphyrin moieties across the MOF crystals as opposed to a kinetically fast process resulting in high porphyrin density at the outer layers of the crystallites. This has been a well-adopted strategy to realize a uniform D-A or related dyad system including [porphyrin-TBAPy] within the MOF crystallites.[22,35,46,47]

Next, we wanted to determine the position of the installed porphyrins, particularly to understand their proximity to the MOF linkers. For this, we performed diffuse reflectance infrared Fourier transform spectroscopy (DRIFTS) and analyzed our data relative to the relevant known systems including the detailed analysis reported by Hupp and co-workers.[43,48,49] In the signature O−H stretching region (i.e., 3800−3600 cm^{-1}) both BFBP(Zn)@NU-1000 and TFP(Zn)@NU-1000 display a single peak at ∼3675 cm^{-1} (Figure 2). Generally, a sharp 3675 cm^{-1} peak is assigned to OH-stretching of the H-bonding-stabilized OH//OH_2 pair from two adjacent Zr-centers that is achieved in so-called "locked" SBUs with more than eight carboxylates bridging the adjacent Zr-centers (such as three formate-capped NU-1000 or UiO-66 with low missing-linker defect density of one to three linkers

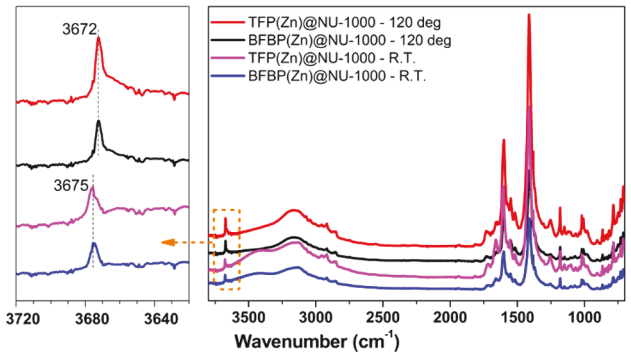

Figure 2. DRIFT spectra of porphyrin@NU-1000 compositions collected at room temperature (RT) and 120 °C, highlighting the O−H stretching characteristics of the H-bonding-stabilized OH//OH_2 pair of "locked" 8-connected Zr_6-oxo SBUs achieved in μ_2−η^2 carboxylate bridging of two adjacent Zr ions.

https://doi.org/10.1021/jacs.1c06629
J. Am. Chem. Soc. 2021, 143, 15286−15297

per node). These H-bonding-stabilized aqua ligands are stable and more difficult to remove even at 120 °C. In contrast, the 8-connected SBUs, free of any other $\mu_2-\eta^2$ carboxylate bridging, would display a broad peak centering at 3657 cm^{-1} (see Figure S7) stemming from four pairs of OH//OH_2 that are not H-bonded and therefore readily lose the aqua ligands, displaying a new peak at 3780 cm^{-1} from the isolated OH.[50] Both BFBP(Zn)@NU-1000 and TFP(Zn)@NU-1000 samples did not show this spectral feature, except that the 3675 cm^{-1} peak became more narrow and shifted to 3672 cm^{-1} at 120 °C, possibly by a reduced heterogeneity of the average OH/OH_2 ligands (as only one of a total of eight available open sites, over two nodes, is capped by a porphyrin carboxylate in our samples). On the basis of these observations, we determined that the carboxy-appended porphyrins are bound in the $\mu_2-\eta^2$ mode (bridging two adjacent Zr-centers).[51]

To further elucidate the binding motif of the carboxy-appended porphyrins at the SBUs, we prepared NU-1000 single-crystals (~50 μm; see Figure S1 for the characterization data) that were similarly functionalized with BFBP(Zn)-COOH and TFP(Zn)-COOH. The obtained samples named BFBP(Zn)@NU-1000(SC) and TFP(Zn)@NU-1000(SC) were mounted for single-crystal X-ray diffraction data collection. While the solved structure did not show sufficient electron density from the nonperiodically[52] installed porphyrins, it did provide key evidence, in terms of the distance between the terminal oxygen atoms from the adjacent Zr(IV) centers [i.e., $d_{(Zr1)O-O(Zr2)}$], indicating that the porphyrin is leveraged through a $\mu_2-\eta^2$-type carboxy-node attachment. In general, NU-1000 SBU (Zr_6-oxo node with 8 phenyl-carboxylates from the TBAPy linkers) will have four pairs of OH//OH_2 with $d_{(Zr1)O-O(Zr2)}$ = 3.3 (±0.1 Å) (Figure 3b). In contrast, the SBU of formate-capped NU-1000 will render a shorter $d_{(Zr1)O-O(Zr2)}$ (2.4 ± 0.1 Å) (Figure 3a). Of these four pairs of OH//OH_2 or carboxy binding sites, two are protruding to two adjacent hexagonal mesopores that are sharing the node and are suitable to host a large porphyrin in a $\mu_2-\eta^2$ type carboxy-node attachment involving two adjacent Zr-atoms (Figure 3c,d). This is supported by the measured $d_{(Zr)O-O(Zr)}$ = 3.13 Å for the pair of terminal O atoms that are protruding to the hexagonal channel; this distance is the average of $(Zr_1)O-O(Zr_2)$ distances if one in four sites is carboxy-bridged (i.e., [(3.3 × 3) + 2.4]/4). The two unbound sites, directed to the small pores, along the *ac*-direction, remain unchanged (observed $d_{(Zr1)O-O(Zr2)}$ = 3.31 Å; Figure 3c). A similar distance between the terminal O atoms protruding to the hexagonal channel was also measured for the TFP(Zn)@NU-1000 (3.09 Å). The SC-diffraction and the DRIFTs data are consistent with for $\mu_2-\eta^2$-type carboxy-bridged attachment of the porphyrins. Carboxy-appended functional groups whose conjugate bases are not sufficiently basic (e.g., *p*-nitrobenzoate[34]), or experience a large steric hindrance catered by the linker side-phenyl and the incoming functional group, would prefer a monodentate binding to one Zr^{IV} center instead of two.

Ground-State Electronic Properties. Ground-state (GS) electronic potentials of individual components were determined from electrochemistry. The CV of NU-1000 deposited on a glassy carbon electrode displays TBAPy-centered oxidation and reduction events at +1.35 V and −0.74 V (vs Ag/AgCl) with an electrochemical bandgap of 2.09 V (Figure 4a).[35] An excited-state oxidation potential of −1.75 V was determined for NU-1000 from its optical band gap of 3.10 eV

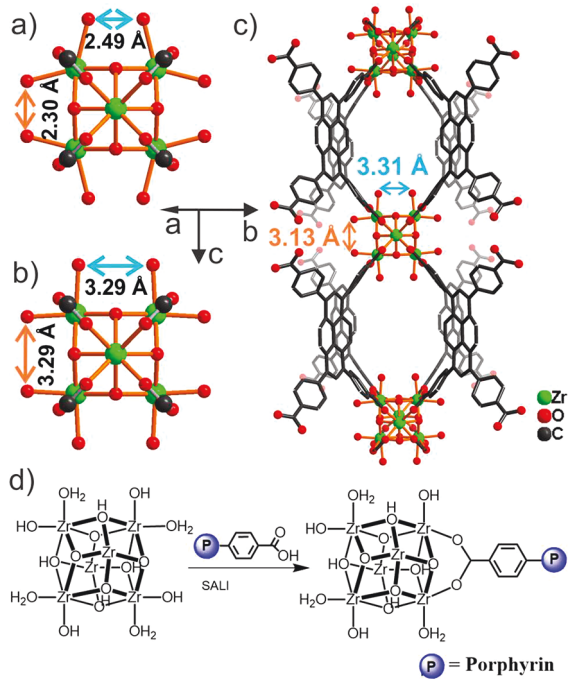

Figure 3. Structure of Zr-oxo SBU extracted from single-crystal XRD data highlighting the distinct $d_{(Zr1)O-O(Zr2)}$ between terminal OH//OH_2 in (a) formate-capped NU-1000, (b) 8-connected SBU without any capping ligand, and (c) BFBP(Zn)@NU-1000. (d) Scheme displaying the SALI process between Zr SBU and carboxy-functionalized porphyrin; note that this acid−base reaction grafts the incoming carboxyporphyrin (in $\mu_2-\eta^2$ bridging mode) at the expense of two water molecules.

(UV−Vis absorption peak at ca. 400 nm; Figures 5a and S9). The ground-state redox potentials determined for BFBP(Zn)-COOEt and TFP(Zn)-COOEt suggest that these compounds possess comparable electrochemical band gaps of ca. 2 eV. Endowed with two more trifluoromethyl groups, TFP(Zn)-COOEt possesses a more positive set of potentials for its first redox events (at −0.62 V and +1.44 V) compared to that of BFBP(Zn)-COOEt appearing at −0.83 V and +1.20 V (Figure 4a). Because these porphyrin compounds also possess an optical bandgap of ca. 2 eV (the Q-band transition of BFBP(Zn)-COOEt and TFP(Zn)-COOEt appears at 603 nm (2.06 eV) and 607 nm (2.05 eV)), their excited-state oxidation potentials are also comparable to their respective ground-state reduction potentials, −0.86 and −0.61 eV, respectively. The relative potential alignment, as summarized in Figure 4b, suggests a thermodynamically favorable EnT from the excited MOF (NU-1000*) to the node-anchored porphyrin species.[35] In contrast, the individual excited-state redox potentials of both of these porphyrin compounds do not implicate a large driving force (ΔE on the order of 0.1 eV) for a PCT involving porphyrin*//NU-1000 ($E_{ox}^{BFBP(Zn)*}$ = −0.86 V against $E_{red}^{NU-1000}$ = −0.74 V for an electron transfer or $E_{red}^{TFP(Zn)*}$ = +1.43 V against $E_{ox}^{NU-1000}$ = +1.35 V for a hole transfer).

The CV of the BFBP(Zn)@NU-1000 composition suggests that components are not electronically coupled at their ground state, as the first oxidation appears at ca. +1.2 V corresponding to the node-bound BFBP(Zn) and at −0.74 V for MOF reduction; we note that peaks for the second and/or third redox events will be kinetically impacted by permselective diffusion of the counterions.[35,53] In contrast, the electrochemistry of TFP(Zn)@NU-1000 is highlighted by a broad

https://doi.org/10.1021/jacs.1c06629
J. Am. Chem. Soc. 2021, 143, 15286−15297

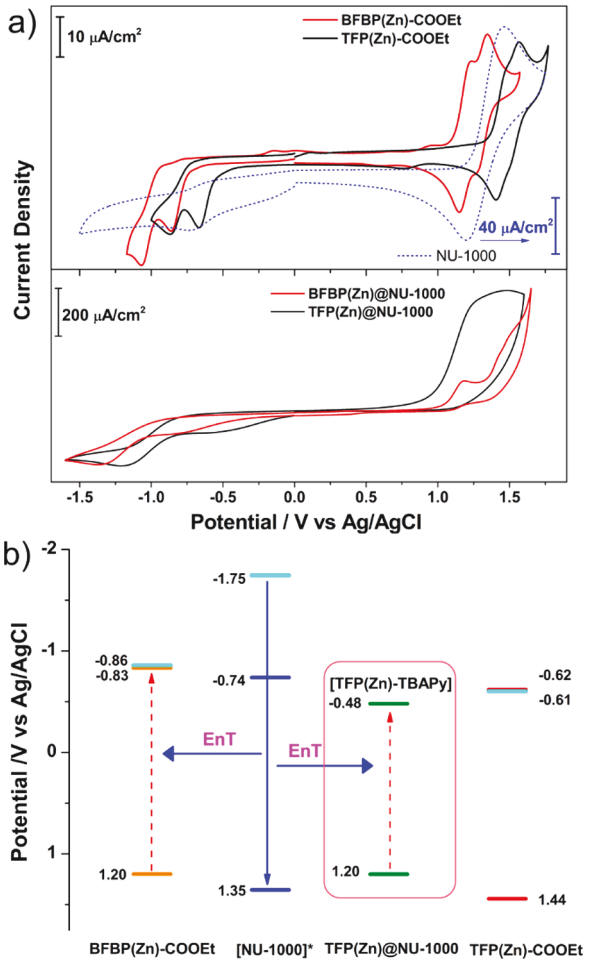

Figure 4. (a) Cyclic voltammograms of individual component: unmodified NU-1000 and carboxy-appended porphyrins (top) and porphyrin@NU-1000 compositions (bottom). (b) Experimentally determined ground- and excited-state potentials of NU-1000 and porphyrins as well as the TFP(Zn)@NU-1000 composition; the excited-state oxidation potentials are shown in cyan.

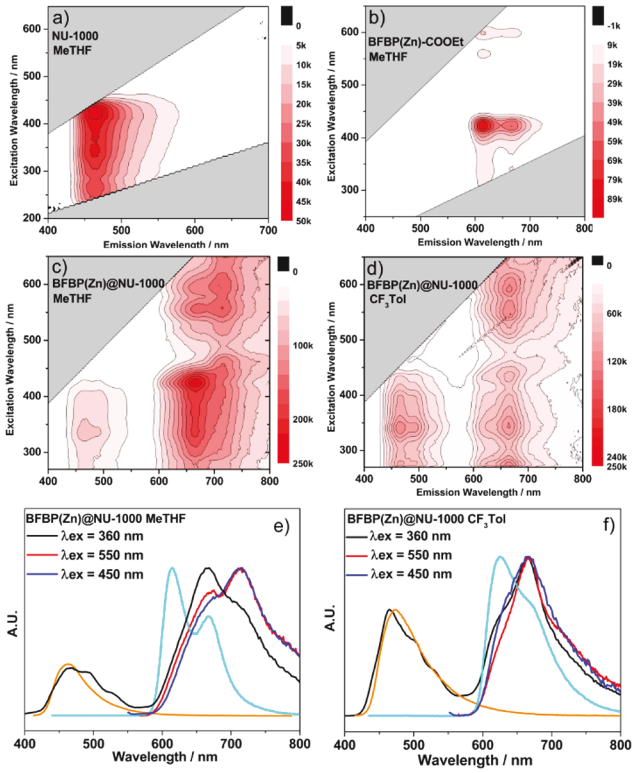

Figure 5. Excitation and emission mapping spectra of (a) NU-1000, (b) BFBP(Zn)-COOEt, and (c) BFBP(Zn)@NU-1000 collected in MeTHF. (d) BFBP(Zn)@NU-1000 collected in CF_3Tol solvent. Emission scans of BFBP(Zn)@NU-1000 relative to BFBP(Zn)-COOEt (cyan) and NU-1000 (orange) components at various excitation wavelengths are presented in (e) MeTHF and (f) CF_3Tol solvents.

oxidative wave with the first oxidative event occurring at a lower potential (+1.2 V) compared to the individual potentials measured for both NU-1000 and TFP(Zn)-COOH components (Figure 4a,b). Despite a relatively low concentration of porphyrins within the framework, a significantly large current density was observed through the entire +1.2 to +1.55 V range; this suggests an improved charge conductivity of an electronically mixed [TFP(Zn)-TBAPy] ground state. Such behavior was theoretically and experimentally shown with fullerene- or carborane-filled NU-1000 and PCN-222 MOFs.[54−56]

Steady-State Spectroscopy. Steady-state excitation/emission mapping spectra (EEMS; Figure 5a−d, Figures S8 and S15) for the hybrid and the respective individual components were collected in MeTHF and CF_3Tol solvents (these solvents were chosen based on their varying solvent dielectric constant with comparable dispersity). The EEMS plots for NU-1000 and BFBP(Zn)-COOEt in MeTHF (Figure 5a,b) highlight their excitation/emission profile maximized at 410/465 nm and 420/620−660 nm, respectively. In contrast, the EEMS plot for BFBP(Zn)@NU-1000 displays two manifolds; one is NU-1000-centric, which appears with a relatively narrow spectral envelope with significantly diminished intensity (QY ∼ 0.35% relative to 42% for the unfunctionalized NU-1000) peaking at 350/460 nm (Figure 5c,d), relative to NU-1000 at 410/465 nm. The porphyrin-centric manifold has also gone through a profound makeover: first, the excitation profile now includes that of NU-1000 (i.e., 300−420 nm) going beyond its original 420 nm Soret peak; second, the porphyrin-centric emission envelope was broadened with a new peak appearing at 710 nm (in addition to the original 620 and 660 nm peaks, Figure 5c−f). A weak MOF-centric emission and the relative energy level alignment of the components suggest a thermodynamically favorable energy transfer from NU-1000* to BFBP(Zn). However, it is not clear if the EnT occurs through a Förster resonance energy transfer (FRET) process or an excited-state complex formation, given that a broad, solvent dielectric-responsive excitation/emission (ex/em) (300−420/610−750 nm; Figure 5c−f) profile is observed (vide infra; see time-resolved spectroscopy). We also note that this low-energy porphyrin-centric profile is different from what was seen for the TPP(Zn)@NU-1000 system, which manifested a solvent dielectric-dependent porphyrin emission envelope without spectral line broadening or the appearance of any new peak. Nevertheless, if the NU-1000* population quenching (measured by its diminished QY) in this hybrid is solely due to EnT, through FRET or excited-complex formation, it must be efficient with a rate constant in the range of 1×10^{11} s^{-1} ($\tau \sim 10 \pm 1$ ps; see SI section G).

In contrast, TFP(Zn)@NU-1000 displays an EEMS plot (Figure S8) with two manifolds, a diminished MOF-centered emission (QY ∼ 0.28% compared to a 42% in pristine NU-

https://doi.org/10.1021/jacs.1c06629
J. Am. Chem. Soc. 2021, 143, 15286−15297

1000) and a broad, structureless porphyrin-centered envelope peaking at 660 nm. The entire excitation profile and the emission spectral envelope do not seem to be sensitive to solvent dielectrics. Considering the ground-state electrochemical feature, discussed earlier, an electronically coupled [TFP(Zn)−TBAPy] dyad is attributed to this spectral behavior. This dyad, with a lower bandgap, is serving as an energy trap/acceptor (i.e., an EnT from NU-1000* to [TFP(Zn) −TBAPy], and based on the QY reduction of NU-1000*, a rate constant $k_{EnT} = 2 \times 10^{11}$ s^{-1} can be estimated) and thereby diminishing the MOF emission. The rest of the emission profile is dominated by the excited-state feature of this low-energy dyad. This postulation can be verified from a short TFP(Zn)−TBAPy distance in TFP(Zn)@NU-1000 (Figure S23): due to a cradle-shaped conformation of the TFP(Zn) core,[57,58] it can approach closer to the pyrene (relative to a BFBP(Zn) or a TPP(Zn) cores attached similarly at the Zr-SBUs; see some optimized structures in SI section F).

Coming back to the possibility of excited-complex formation, three possibilities can be considered: [NU-1000*−BFBP(Zn)], [BFBP$(Zn)_{S2}$*−TBAPy], and [BFBP$(Zn)_{S1}$*−TBAPy] (the S2 and S1 subscripts denote the Soret- and Q-band-derived excitations of the porphyrin, respectively). These exciplex-like complexes are formed by the electronic interactions between one excited molecule (M_1*) and a ground-state counterpart (M_2).[59] The new excited species, M_1*M_2, commonly feature distinct photophysics from its individual components (M_1* and M_2*); e.g., a red-shifted emission stemming from a stabilized M_1*M_2 state (possibly through an electronic redistribution) along with a longer emissive lifetime can be seen. The ex/em profile of BFBP(Zn)@NU-1000 collected in MeTHF (Figure 5c) suggests that [BFBP$(Zn)_{S1}$*−TBAPy], selectively achieved by exciting in the 500−600 nm region, has a dominant new peak at 710 nm. In contrast, the emission envelope of this hybrid obtained by 300−420 nm excitation does not provide 710 nm emission as a dominant route (Figure 5c); this indicates that the higher-energy species, such as NU-1000* and/or [NU-1000*−BFBP(Zn)], may have other decay channels that do not lead to efficient formation of the low-energy [BFBP$(Zn)_{S1}$*−TBAPy]. This may stem from the different orientations of nondegenerate *x*- and *y*-polarized transition dipoles of this porphyrin, especially when put together within the pores: in other words, the transition dipoles involved in [NU-1000*−BFBP(Zn)] can be different than the one that forms [BFBP$(Zn)_{S1}$*−TBAPy]. The emissive relaxation of the [BFBP$(Zn)_{S1}$*−TBAPy] seems solvent dependent: the dominant peak at 710 nm seen in MeTHF solvent is diminished in CF_3Tol, indicating that this emissive complex may be polar or efficiently relaxes to a polar nonemissive state (like a CT state).

Time-Resolved Emission Spectra. The dynamics of the emissive species were probed with time-resolved emission spectral (TRES) evolution and analyzed with the corresponding transient emissive profiles. Figure 6 highlights the data collected for BFBP(Zn)@NU-1000 in MeTHF and CF_3Tol solvents by 403 nm pulsed laser excitation (IRF ca. 75 ps). Congruent with the steady-state emission profiles, the TRES plots highlight the time evolution of two emission manifolds. The 403 nm excitation initially creates dominating NU-1000* and small BFBP(Zn)* populations (by excitation at the blue tail of its 420 nm excitation/absorption band); this can be seen

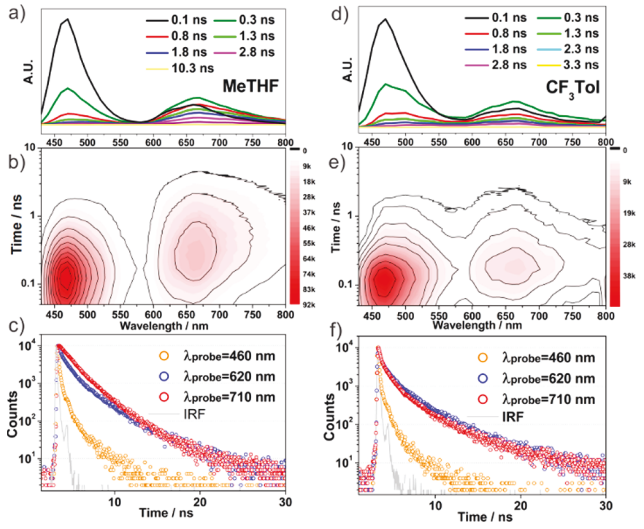

Figure 6. TRES data collected for BFBP(Zn)@NU-1000 in (a−c) MeTHF and (d−f) CF_3Tol solvents upon 403 nm excitation. (a, d) Transient emission spectra at labeled time delays. (b, e) Contour plots showing the time (log scale) evolution of the spectra with intensity (color-coded). (c, f) Transient kinetic profiles probed at various key (labeled) wavelengths.

by the relative intensity of the spectral envelope at the earliest TRES collected in MeTHF solvent (at ∼0.1 ns, Figure 6a,b). While the NU-1000* manifold quickly decays, the porphyrin manifold first grows with an increase in the intensity of the red-side shoulder (relevant to the peak at 710 nm) and then decays. Kinetic analysis of the transient decay profiles (Figure 6c) probed/measured at 460 nm (NU-1000 manifold) suggests a fast decay with $\tau \approx 0.4$ ns (compared to the ∼1 ns lifetime of pristine NU-1000). In contrast, the porphyrin manifold shows slightly different kinetic profiles at its blue and red sides of the emissive spectral envelope: at 620 nm, the major population decays with $\tau \sim 1.1$ ns (65%) whereas at 710 nm, $\tau \sim 1.4$ ns (65%)%); the lifetime data are summarized in Table 1.

TRES data collected in polar CF_3Tol solvent (Figure 6d−f) also showed a similar time evolution of the NU-1000 and porphyrin manifolds, i.e., the initial formation of more NU-1000* with smaller BFBP(Zn)* population; from there, the latter one first grows and then decays but with lower intensity for its red shoulder (compared to TRES evolution recorded in MeTHF; Figure 6a,b). Kinetic analysis of the corresponding transient profiles (Figure 6f) displayed that the NU-1000 manifold showed essentially unchanged decay ($\tau \approx 0.4 \pm 0.05$ ns; Table 1) compared to that seen in MeTHF. However, the kinetics of the porphyrin manifold suggests a slightly faster decay at the red side probed at 710 nm ($\tau \approx 1.0$ ns; ∼65%) compared to its blue side probed at 620 nm ($\tau \approx 1.2$ ns; 65%). This is congruent with the fact that in a highly polar solvent, the emissive state of the [BFBP$(Zn)_{S1}$*−TBAPy] is more effectively relaxed to a nonemissive CT state. Note that overlapping emissive profiles of these two species (i.e., BFBP$(Zn)_{S1}$* and [BFBP$(Zn)_{S1}$*−TBAPy], where the former is the remaining noncomplexed porphyrins; vide infra), limited by the temporal resolution of the TCSPC instrument, did not allow a well-resolved probe of their evolution and decay individually. While the kinetics probed at the 710 nm can be significantly contaminated by the BFBP$(Zn)_{S1}$* emission, the sizable difference in their response to the solvent dielectric (τ

https://doi.org/10.1021/jacs.1c06629
J. Am. Chem. Soc. 2021, 143, 15286−15297

Table 1. Emission Lifetime Data for Por@MOF and Individual Components

	λ_{ex} = 403 nm			λ_{ex} = 507 nm	
compound	τ_{460} (ns)	τ_{620} (ns)	τ_{710} (ns)	τ_{620} (ns)	τ_{720} (ns)
NU-1000	1.0	–	–	–	
BFBP(Zn)-COOEt	–	2.3[a] (2.6[b])	–	2.6[a] (2.8[b])	
TFP(Zn)-COOEt	–	0.8[a,b]	–	1.0[a,b]	
BFBP(Zn)@NU-1000	0.4[a,b,e]	1.1[a,c] (1.2[b,c])	1.4[a,c] (1.0[b,c])	1.1[a,c] (0.6[b,d])	1.5[a,c] (0.6[b,d])
TFP(Zn)@NU-1000	0.2[a,e] (0.5[b,e])	0.7[a,e] (0.7[b,e])	0.9[a,e] (0.9[b,e])	0.8[a,e] (0.7[b,e])	0.9[a,e] 0.9[b]

[a]Data collected in MeTHF solvent. [b]Data collected in CF_3Tol solvent. [c]Major (65−75%) contribution, the residual (25−35%) is contributed by a longer ∼3 ns component. [d]Major (60%) contribution, the residual (40%) is contributed by a longer ∼2.5 ns component. [e]Major (85−90%) contribution, the residual (10−15%) contributed by a longer ∼2.0 ns component.

≈ 1.4−1.0 ns @710 nm; Table 1) compared to the more-or-less solvent-independent blue side ($\tau \approx 1.15 \pm 0.05$ ns; Table 1) supports the existence of two species including a fast-evolving [BFBP(Zn)$_{S1}$*−TBAPy] that decays to polar non-emissive species. For all the transient profiles, the small ca. 35% contribution is coming from a longer 3 ns component. A delayed thermally accessed [BFBP(Zn)$_{S1}$*−TBAPy] from a lower-energy nonemissive CT state can be assigned.

Coming back to the involvement of the EnT for the NU-1000* population decay, the maximum rate constant, estimated from the lifetime data (from the fastest component of ∼0.1 ns), can be in the range of 1×10^{10} s^{-1}, which is about 1 order magnitude slower than that estimated from the QY reduction (vide supra). This suggests that there may be more emission quenching processes in the BFBP(Zn)@NU-1000 composition that is not dynamic in nature. Given the complex relaxation pathways of the higher energy species involving NU-1000* and BFBP(Zn)$_{S2}$*, we wanted to follow the evolution and decay of BFBP(Zn)$_{S1}$*−TBAPy that are derived just from BFBP(Zn)$_{S1}$* (by selective excitation at 507 nm pulsed laser; IRF = 100 ps). Congruent with the steady-state emission profile (Figure 5c,d), the porphyrin-only TRES plots (Figure 7a,b,d,e) highlight broader manifolds than what is observed by 403 nm excitation. Kinetic analysis of the transient decay profiles (Figure 7c,f) probed at 620 and 720 nm in MeTHF solvent also suggests a similar trend and profiles with time constants of 1.1 and 1.5 ns (major component 65%; Table 1). However, TRES data collected in CF_3Tol solvent show a spectral envelope with faster decay profile of 0.6 ns (60%) for both the blue and red sides (i.e., 620 and 720 nm, respectively). This faster decay time (0.6 ns) is in line with a facile relaxation of [BFBP(Zn)$_{S1}$*−TBAPy] to a nonemissive CT state in a polar solvent (than in MeTHF), where a slow formation of BFBP(Zn)$_{S1}$* did not contribute at 507 nm excitation. These transient profiles are also contributed by a delayed component (2.5 ns; ∼40%) stemming from a nonemissive state through delayed thermal equilibration. On the basis of the emissive-spectra and their time-resolved evolutions, we can conclude that a low-energy exciplex-like emissive intermediate, [BFBP(Zn)$_{S1}$*−TBAPy], is forming, starting from an initially created BFBP(Zn)$_{S1}$* by direct excitation or from higher energy species such as NU-1000* and BFBP(Zn)$_{S2}$* through [NU-1000*−BFBP(Zn)] and fast internal conversion (IC), respectively. The low-energy [BFBP-(Zn)$_{S1}$*−TBAPy] complex eventually relaxes to a polar nonemissive CT-type species. Some of these decay processes occur on a time scale faster than the instrumental detection limit (e.g., porphyrin $IC_{S2\rightarrow S1}$ with $\tau \lesssim 0.18$ ps). Nevertheless, we note from the decay time of NU-1000* that NU-1000-centric excitation (300−400 nm) provides slow (ca. 100 ps time scale) formation of BFBP(Zn)$_{S1}$* and therefore an EnT through [NU-1000*−BFBP(Zn)] complexation can be considered. This is because a FRET, measured for TPP(Zn)@NU-1000 with a similar driving force, at this distance is fast, τ = ∼2 ps.[60]

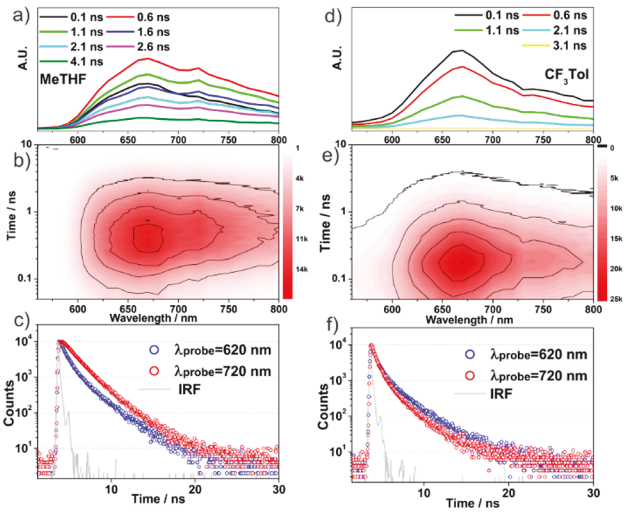

Figure 7. TRES data collected for BFBP(Zn)@NU-1000 in (a−c) MeTHF and (d−f) CF_3Tol solvents upon selective Q-band-derived (507 nm) excitation. (a, d) Transient emission spectra at labeled time delays. (b, e) Contour plots showing the time (log scale) evolution of the spectra with intensity (color-coded). (c, f) Transient kinetic profiles probed at various key (labeled) wavelengths.

In contrast, the TRES and the corresponding kinetic profiles (Figures S13 and S14) for TFP(Zn)@NU-1000 do not show much dielectric or excitation wavelength dependence. The TRES plot (Figure S13b,e) highlights NU-1000 and porphyrin-centric manifolds. The NU-1000*-centric emission envelope (including its QY) shows a dramatic reduction due to the population decays through an efficient EnT (NU-1000* → [TFP(Zn)−TBAPy]), where the time evolution of the structureless porphyrin-centric emission manifold is the property of the low-energy [TFP(Zn)−TBAPy]* (i.e., the excited state of the bimolecular complex formed at the ground state) with a time constant of 0.8 ± 0.1 ns, which is comparable to the lifetime for pristine TFP(Zn)-COOEt (see Table 1).

Transient Absorption Spectroscopy. Femtosecond transient absorption (fs-TA) spectra of BFBP(Zn)@NU-1000 were acquired by exciting the sample dispersed in MeTHF solvent at 400 nm. Due to the complex nature of the TA-spectral evolution, the raw fs-TA spectra are presented in three segments (Figure 8): early time (before 1.3 ps), mid time

https://doi.org/10.1021/jacs.1c06629
J. Am. Chem. Soc. 2021, 143, 15286−15297

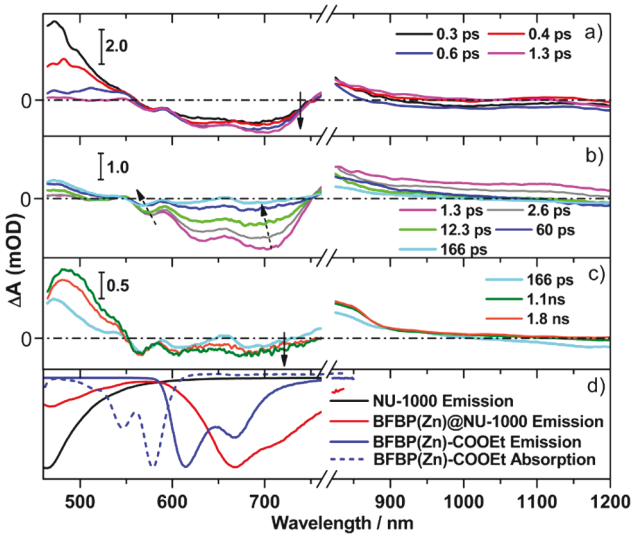

Figure 8. Representative femtosecond transient absorption (fs-TA) spectra for BFBP(Zn)@NU-1000—for clarity, presented in three time-domains. Experimental condition: suspension in MeTHF solvent; λ_{ex} = 400 nm; fluence = ~280 μJ/cm^2. Panel d displays relevant inverted steady-state spectra of BFBP(Zn)@NU-1000 compositions and their components for comparison for fs-TA spectra.

(1.3 < t < 170 ps), and late stage (170 ps < t < 2.5 ns). The early time evolution is marked with an excited-state absorption (ESA) of BFBP(Zn)$_{S1\rightarrow Sn}$* centering at 470 nm, which slowly diminishes with the increase in stimulated emission (SE) at 620 and a low-energy peak at ~700 nm stemming from the [BFBP(Zn)$_{S1}$*−TBAPy] exciplex-like species. The 700 nm negative peak is broad, contributed from a 670 nm SE shoulder of the BFBP(Zn)*, and a blue-shift (from its 720 nm peak) caused by the NU-1000*$_{S1\rightarrow Sn}$ ESA at 740 nm. The reduction of ESA peak intensity for BFBP(Zn)$_{S1\rightarrow Sn}$ at 460 nm is not tied with the SE from NU-1000*, as it also should decrease over time. The mid time (1.3 < t < 166 ps) evolution is highlighted by the rise of an ESA peak at ~480 nm and reduction of the SE with the red side decaying faster (leading to a blue shift of the 700 nm peak to 674 nm). The ground-state bleaching (GSB) band that originally appeared at ~580 nm was also reduced and blue-shifted to 565 nm. We assign this time evolution associated with relaxation of the low-energy exciplex-like complex and formation of the CT-type complex (see below). The late stage is dominated by a spectral feature that is mixed with CT- and porphyrin- triplet character.

Given a small difference in their redox potentials (Figure 4b), ΔG^0 for electron transfer from BFBP(Zn)* to TBAPy (NU-1000) LUMO is −0.28 eV and that for a hole transfer (i.e., an electron from the ground-state TBAPy HOMO (or NU-1000 HOCO) being transferred to BFBP(Zn)*) is −0.1 eV (see SI section G). While this estimation uses the potentials for the individual components, the excited-state energy, especially in an exciplex-like "bound" state, may be lower (by ~0.1 eV). This estimation also accounts for the optimized ground-state structure where a center-to-center distance between BFBP(Zn) and the closest TBAPy is ~11 Å. In a solvated exciplex-like "bound" state, the distance between porphyrin and adjacent linker can be shorter which will improve the driving force. Therefore, from a higher driving force argument, we can expect that a CT complex, [BFBP-(Zn)$^{\bullet+}$−TBAPy$^{\bullet-}$], should form from [BFBP(Zn)$_{S1}$*−TBAPy]. The ESA associated with TBAPy$^{\bullet-}$ that appears at ~600 nm is obscured by the GSB and the blue tail of the 620 nm SE peak. The time evolution (midrange; Figure 8b) displays a ~580 → 565 nm blue shift of the GSB. This is accompanied by the appearance of a broad ESA peak at ~820 nm (blue spectrum in Figure 8b at 60 ps delay time).

The fs-TA spectral data were fit into a three-species target model (**A** → **B** → **C**) yielding species-associated spectra (SAS), shown in Figure 9 along with time-resolved species

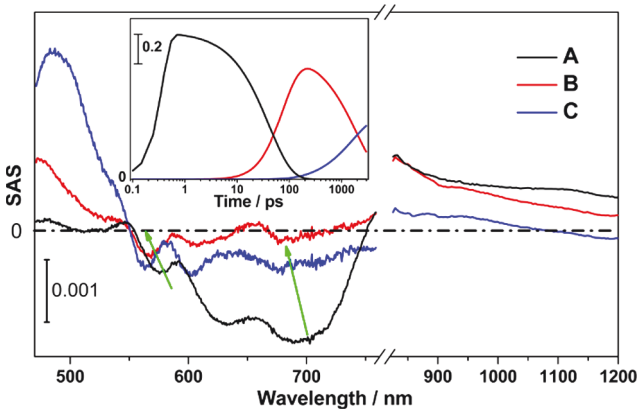

Figure 9. The SAS of fs-TA data for BFBP(Zn)@NU-1000. Inset is the state-associated population evolution of BFBP(Zn)@NU-1000.

population kinetics. Given the complexity of the system and the inherent scattered nature of the TA data, we note that SAS are likely to reflect signals arising from multiple species rather than discrete individual ones.[36] As discussed above, the [BFBP(Zn)$_{S1}$*−TBAPy] state is assigned to species **A** in SAS (Figure 9), bearing a low-energy emission band at 700 nm. The corresponding SAS (black spectrum in Figure 9) is contaminated by BFBP(Zn)$_{S1}$* with its 628 nm SE, which means there must also be some contribution from the BFBP(Zn)$_{S1\rightarrow Sn}$ transition centering at 460 nm. Therefore, the actual SAS of [BFBP(Zn)$_{S1}$*−TBAPy] should have a negative band in the ~450−470 nm region.[61] The population dynamics (Figure 9 inset) suggest that species **A** forms before 1 ps with a time constant of ~0.3 ps. Ultrafast IC of BFBP(Zn)*$_{S2\rightarrow S1}$ (<180 fs) precludes a direct spectral probe if the low-energy [BFBP(Zn)$_{S1}$*−TBAPy] complex is formed from a BFBP(Zn)$_{S1}$* or BFBP(Zn)$_{S2}$* through [BFBP-(Zn)$_{S2}$*−TBAPy]. However, from the initial presence and fast decay of BFBP(Zn)$_{S1\rightarrow Sn}$ ESA peak at 470 nm, we can say that the low energy exciplex is preceded by the porphyrin IC$_{S2\rightarrow S1}$ (and not through [BFBP-(Zn)$_{S2}$*−TBAPy]). Species **A** has a lifetime of 120 ps which is a combined rate of its decay to a polar CT state of species **B** (with τ = 44 ps) and its radiative decay to the ground state (τ = 540 ps). This emissive decay time scale is within the range that was extracted by kinetic analysis of the transient emissive decay profiles at λ_{ex} = 507 nm (τ_1 = 0.6 ns; Figure 7a, Table 1). The relevant rate constants in terms of lifetimes are presented in Figure 10, where the GTA modeling data are boxed in a dotted line.

Species **B** is efficiently formed (τ = 44 ps) possibly, at least partly, due to its structural similarity with species **A** and therefore involving a small internal reorganization energy and a lower barrier ($\Delta G^{\ddagger}$). Species **B** is a relatively long-lived species (τ = 2 ns) that undergoes a branched decay to triplet species **C** and thermal charge recombination to the ground state (τ = 2.2

https://doi.org/10.1021/jacs.1c06629
J. Am. Chem. Soc. 2021, 143, 15286−15297

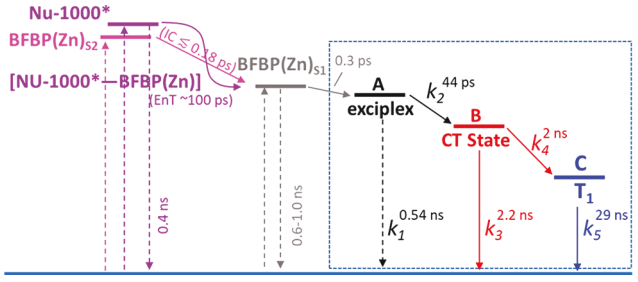

Figure 10. Rate constants for the excited-state species, obtained from various time-resolved data including the simulated kinetic model of the fs-TA (dotted box). The electronic excitation and radiative decays are shown with dashed arrows.

ns). The SAS of species **B** displays a blue-shifted, 565 nm, GSB and a broad ESA near the 800 nm region (red spectrum in Figure 9a). The remaining question, in the early mid time evolution, is the involvement and the fate of NU-1000* in BFBP(Zn)@NU-1000. The fs-TA data does not provide much information, as the spectral signatures of the NU-1000-centered GSB (at ∼400 nm), SE (at ∼450), and $S_1 \rightarrow S_n$ (at 740 nm) are obscured either by the excitation-scattering or other dominant signals stemming from $BFBP(Zn)_{S1}$* and [$BFBP(Zn)_{S1}$*−TBAPy]. However, we can revisit the EnT-driven emission quenching of NU-1000* population within tens of picoseconds time scale and the fact that the NU-1000 excitation (at 320−400 nm) produced a smaller amount of [$BFBP(Zn)_{S1}$*−TBAPy] compared to a Q-band-based excitation; based on these, we can infer that NU-1000* has provided a steady population of BPBF(Zn)* through FRET and/or through [NU-1000*−BFBP(Zn)] complex formation. Because a FRET-based EnT from NU-1000* is fast ($\tau \sim 2$ ps),[35] there may be two possible routes to form the low-energy [$BFBP(Zn)_{S1}$*−TBAPy] exciplex-like intermediate: one relatively dominant (fast) route starting from $BFBP(Zn)_{S2}$* and going through $BFBP(Zn)_{S1}$* via $IC_{S2\rightarrow S1}$ occurring within 1 ps, and the other route starting from NU-1000*, possibly through [NU-1000*−BFBP(Zn)], as the rate-limiting step over tens of picoseconds, forming $BFBP(Zn)_{S1}$* via energy transduction within the high-energy complex.

Species **C** is believed to be formed through intersystem crossing (ISC; τ = 2 ns). On the basis of the relative energetics, we do not expect that the CT species (**B**) relaxes to individual components. A direct ISC[36] leaves an open question on the involvement of TBAPy in this triplet-state species. The spectral signature of **C** (Figure 9a or a late-stage spectrum in Figure 8c) indicates a good match with the ^{3}BFBP(Zn)* with ESA at 477 nm and broad NIR $T_1 \rightarrow T_n$ transitions along with a bleaching signature at 565 and 610 nm, similar to pure BFBP(Zn)-COOEt measured in solution (Figure S20). We believe that the energetic cascade in the triplet manifold deserves a separate set of investigations addressing such key questions.

The fs-TA spectra of TFP(Zn)@NU-1000, collected in MeTHF solvent by 400 nm excitation (Figure 11a−c), highlight the spectral evolution of the [TFP(Zn)−TBAPy]* species. The low-energy [TFP(Zn)−TBAPy] is formed at the ground state through electronic interaction. Therefore, the early time fs-TA spectra simply display fast energy transfer from the initially formed higher energy species such as NU-1000* and some $TFP(Zn)_{S2}$* that is protruding outward (at the exterior surface) and entail a spectral signature of an individual chromophore. The $TFP(Zn)_{S1\rightarrow Sn}$ ESA peak at

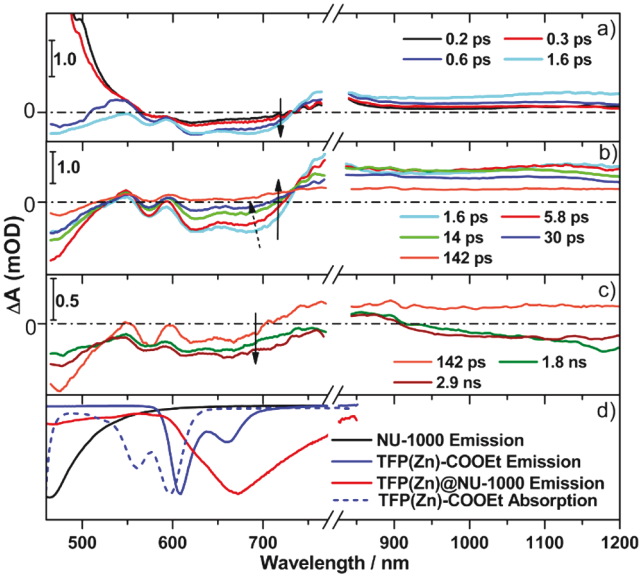

Figure 11. Representative fs-TA spectra for TFP(Zn)@NU-1000, for clarity, presented in three time-domains. Experimental conditions: suspension in MeTHF solvent; λ_{ex} = 400 nm; fluence = ∼280 μJ/cm^2. Panel d displays relevant inverted steady-state spectra of TFP(Zn)@NU-1000 compositions and their components for comparison for fs-TA spectra.

∼470 nm can thus be seen from these exterior TFP(Zn) species at the early time (<0.6 ps). However, once the energy is transferred to the [TFP(Zn)−TBAPy] populating its excited-state species, the entire spectral manifold displays the signature of the [TFP(Zn)−TBAPy]* species: a GSB at 575 and 622 nm which does not show any shift over time and therefore provides a clue that no TBAPy-centered radial ion forms (at ∼600 nm). [TFP(Zn)−TBAPy]* also features a broad ESA envelope from 750 nm and stretching beyond 1200 nm. The other noteworthy features include a broad SE band appearing at 692 nm which slowly blue shifts to 670 nm possibly due to a growing triplet species which has a broad transition ∼800 nm. The negative signal at ≲450 nm stayed throughout; its intensity and width must have been impacted by the SE of NU-1000* and the GSB of any TFP(Zn)* at the earlier time. We believe this ∼450 nm negative band is the GSB of the [TFP(Zn)−TBAPy] complex, appearing at slightly lower in energy than its individual components (Figure 11d), NU-1000 (∼400 nm) and TFP(Zn) (425 nm). Therefore, the spectral signature of the long-lived triplet species, as seen in the late-stage fs-TA data (Figure 11c), is not like that seen for ^{3}TFP(Zn)* (Figure S21); i.e., the $T_1 \rightarrow T_n$ transition centering at 500 nm is missing. Unlike BFBP(Zn)@NU-1000, the fs-TA data for TFP(Zn)@NU-1000 fits into a two species (**A** → **B**) target model revealing one singlet species (**A**) that radiatively relaxes to ground state with 0.67 ns, which is similar to the emissive lifetime and populates its triplet states (over 1.1 ns through ISC; see SI Figure S24). This suggests that species A is the excited state of the ground-state complex [TFP(Zn)−TBAPy].

CONCLUSIONS

In this work, we established a strategy to emulate LHC in a MOF where the tetraphenyl pyrene-derived linker assembly of the host MOF serves as the LH-antenna. The absorbed energy is transferred to electrochemically comparable porphyrins

https://doi.org/10.1021/jacs.1c06629
J. Am. Chem. Soc. 2021, 143, 15286−15297

grafted at its node, which then drive a charge-separation through an exciplex-like [BFBP(Zn)$_{S1}$*−TBAPy] intermediate. Two zinc porphyrins, BFBP(Zn)−COOH and TFP(Zn)−COOH, with similar electrochemical bandgaps were prepared; based on the varying number of trifluoromethyl groups at the meso position of the porphyrins, their redox potentials were tuned within 0.1 V relative to the MOF. The DRIFTS and single-crystal diffraction data collected for the SALI-installed BFBP(Zn)@NU-1000 and TFP(Zn)@NU-1000 suggest that the porphyrins are grafted through μ_2−η^2 type attachment where the carboxy functionality of the incoming porphyrin bridges two adjacent Zr-ions of a node. For BFBP(Zn)@NU-1000, by virtue of their ground- and excited-state potentials, NU-1000* can transduce its absorbed energy to form BFBP(Zn)$_{S1}$*, which entails a long-lived charge-separated complex formed through an exciplex-like [BFBP(Zn)$_{S1}$*−TBAPy] intermediate. This low-energy exciplex is formed within 1 ps and relaxes to a [BFBP(Zn)$^{\bullet+}$−TBAPy$^{\bullet-}$] CT complex with 44 ps time constant. Various time-resolved spectroscopic data suggest that energy transfer from NU-1000* may not involve a fast Förster resonance energy transfer (FRET) but through a slow [NU-1000*−BFBP(Zn)] intermediate formation. The key BFBP(Zn)$_{S1}$* can also be efficiently populated through a direct Q-band excitation (510−570 nm) or through a Soret band excitation (400−430 nm); the latter will involve a fast $S_2 \rightarrow S_1$ internal conversion (IC; τ < 180 fs). The NU-1000* however can maintain a steady flow of the BFBP(Zn)$_{S1}$* over 100 ps. The exciplex-like [BFBP(Zn)$_{S1}$*−TBAPy] intermediate is emissive, and the energy gap with the CT complex [BFBP(Zn)$^{\bullet+}$−TBAPy$^{\bullet-}$] may be low. This arrangement causes a solvent polarity-dependent emission of the [BFBP(Zn)$_{S1}$*−TBAPy] intermediate which, on the other hand, can be thermally accessed back from the lower energy CT complex. Nevertheless, a panchromatic excitation, ranging from 350 to 600 nm, will lead to [BFBP(Zn)$^{\bullet+}$−TBAPy$^{\bullet-}$] through an exciplex formation. Based on the relative decay time constants for this exciplex-like species, the CT formation is more prevalent (τ = 44 ps) than its radiative decay (τ = 0.55 to 1 ns). The results also suggest that driving PCT with a small ΔG^0 not only requires fine-tuning the respective potentials but also an appropriate assembly. Commonly, increasing the number of trifluoromethyl groups hampers porphyrin ring planarity; thus, a cradle-shaped TFP(Zn) comes close to making a ground-state [TFP(Zn)−TBAPy] complex characterized by electrochemical redox events occurring at potentials lower than that of both components. Such low bandgap species serve as an energy trap without the desired PCT. Note, however, if transducing energy for other purposes such as driving ^{3}porphyrin*-sensitized photochemistry, this could be a candidate composition for development. The EnT and PCT events in BFBP(Zn)@NU-1000 are somewhat similar to that seen in natural LHC in PSII. The EnT from LH1 to the special-pair reaction center (RC) commences over ∼30 ps followed by a fast charge separation (CS) within 2 ps, which eventually forms an [RC+ (quinone)-] "trapped" charge-separated state over 200 ps in PSII.[62,63] In BFBP(Zn)@NU-1000, the MOF antenna transfers its energy, similarly, over a tens of picoseconds time scale and the exciplex is formed within 1 ps, leading to a long-lived CT species. Overall, this study shows a strategy to build out a low-density LHC system to generate charge carriers with high potentials and therefore should be appealing to various photoelectrochemical developments.

■ ASSOCIATED CONTENT

Supporting Information

The Supporting Information is available free of charge at https://pubs.acs.org/doi/10.1021/jacs.1c06629.

Experimental details and computational and spectroscopic data (PDF)

■ AUTHOR INFORMATION

Corresponding Author

Pravas Deria − *School of Chemical and Biomolecular Science, Southern Illinois University, Carbondale, Illinois 62901, United States;* orcid.org/0000-0001-7998-4492; Email: pderia@siu.edu

Authors

Xinlin Li − *School of Chemical and Biomolecular Science, Southern Illinois University, Carbondale, Illinois 62901, United States*

Jierui Yu − *School of Chemical and Biomolecular Science, Southern Illinois University, Carbondale, Illinois 62901, United States*

Zhiyong Lu − *Department of Chemistry, Northwestern University, Evanston, Illinois 60208, United States; College of Mechanics and Materials, Hohai University, Nanjing 210098, P. R. China;* orcid.org/0000-0001-8263-8152

Jiaxin Duan − *Department of Chemistry, Northwestern University, Evanston, Illinois 60208, United States;* orcid.org/0000-0003-3252-7870

H. Christopher Fry − *Center for Nanoscale Materials, Argonne National Laboratory, Lemont, Illinois 60439, United States;* orcid.org/0000-0001-8343-5189

David J. Gosztola − *Center for Nanoscale Materials, Argonne National Laboratory, Lemont, Illinois 60439, United States;* orcid.org/0000-0003-2674-1379

Karan Maindan − *School of Chemical and Biomolecular Science, Southern Illinois University, Carbondale, Illinois 62901, United States*

Sreehari Surendran Rajasree − *School of Chemical and Biomolecular Science, Southern Illinois University, Carbondale, Illinois 62901, United States*

Complete contact information is available at: https://pubs.acs.org/10.1021/jacs.1c06629

Notes

The authors declare no competing financial interest.

■ ACKNOWLEDGMENTS

P.D. gratefully acknowledges funding from the National Science Foundation (NSF CAREER CHE-1944903). X.L. acknowledges the B. & M. Gower fellowship (School of Chemical and Biomolecular Science) and dissertation research award through the graduate school at SIUC. Z.L. acknowledges the support from the China Scholarship Council (CSC) (201806715039) during his visit to Northwestern University. J.D. acknowledges the support from the U.S. Department of Energy, Office of Science, Office of Basic Energy Sciences via grant DE-FG02-87ER13808. This work made use of the J. B. Cohen X-ray Diffraction Facility supported by the MRSEC program of the National Science Foundation (DMR-1121262) at the Materials Research Center of Northwestern University and the Soft and Hybrid Nanotechnology Experimental (SHyNE) Resource (NSF NNCI-1542205). SEM-EDS data

were collected at SIUC IMAGE Center (supported by NSF grant no. CHE0959568). Use of the Center for Nanoscale Materials, an Office of Science user facility, was supported by the U.S. Department of Energy, Office of Science, Office of Basic Energy Sciences, under contract no. DE-AC02-06CH11357.

REFERENCES

(1) Scholes, G. D.; Fleming, G. R.; Olaya-Castro, A.; van Grondelle, R. Lessons from Nature About Solar Light Harvesting. *Nat. Chem.* **2011**, *3*, 763−774.
(2) Miller, R. A.; Presley, A. D.; Francis, M. B. Self-Assembling Light-Harvesting Systems from Synthetically Modified Tobacco Mosaic Virus Coat Proteins. *J. Am. Chem. Soc.* **2007**, *129*, 3104−3109.
(3) Damjanović, A.; Ritz, T.; Schulten, K. Energy Transfer between Carotenoids and Bacteriochlorophylls in Light-Harvesting Complex II of Purple Bacteria. *Phys. Rev. E: Stat. Phys., Plasmas, Fluids, Relat. Interdiscip. Top.* **1999**, *59*, 3293−3311.
(4) Barber, J.; Andersson, B. Revealing the Blueprint of Photosynthesis. *Nature* **1994**, *370*, 31−34.
(5) Wasielewski, M. R. Photoinduced Electron Transfer in Supramolecular Systems for Artificial Photosynthesis. *Chem. Rev.* **1992**, *92*, 435−461.
(6) Wasielewski, M. R. Self-Assembly Strategies for Integrating Light Harvesting and Charge Separation in Artificial Photosynthetic Systems. *Acc. Chem. Res.* **2009**, *42*, 1910−1921.
(7) Prathapan, S.; Johnson, T. E.; Lindsey, J. S. Building-Block Synthesis of Porphyrin Light-Harvesting Arrays. *J. Am. Chem. Soc.* **1993**, *115*, 7519−7520.
(8) Hasobe, T.; Kashiwagi, Y.; Absalom, M. A.; Sly, J.; Hosomizu, K.; Crossley, M. J.; Imahori, H.; Kamat, P. V.; Fukuzumi, S. Supramolecular Photovoltaic Cells Using Porphyrin Dendrimers and Fullerene. *Adv. Mater.* **2004**, *16*, 975−979.
(9) Sengupta, S.; Würthner, F. Chlorophyll J-Aggregates: From Bioinspired Dye Stacks to Nanotubes, Liquid Crystals, and Biosupramolecular Electronics. *Acc. Chem. Res.* **2013**, *46*, 2498−2512.
(10) Kim, D.; Osuka, A. Directly Linked Porphyrin Arrays with Tunable Excitonic Interactions. *Acc. Chem. Res.* **2004**, *37*, 735−745.
(11) Feng, D.; Gu, Z.-Y.; Li, J.-R.; Jiang, H.-L.; Wei, Z.; Zhou, H.-C. Zirconium-Metalloporphyrin Pcn-222: Mesoporous Metal−Organic Frameworks with Ultrahigh Stability as Biomimetic Catalysts. *Angew. Chem., Int. Ed.* **2012**, *51*, 10307−10310.
(12) Mondloch, J. E.; Bury, W.; Fairen-Jimenez, D.; Kwon, S.; DeMarco, E. J.; Weston, M. H.; Sarjeant, A. A.; Nguyen, S. T.; Stair, P. C.; Snurr, R. Q.; Farha, O. K.; Hupp, J. T. Vapor-Phase Metalation by Atomic Layer Deposition in a Metal−Organic Framework. *J. Am. Chem. Soc.* **2013**, *135*, 10294−10297.
(13) Jiang, H.-L.; Feng, D.; Wang, K.; Gu, Z.-Y.; Wei, Z.; Chen, Y.-P.; Zhou, H.-C. An Exceptionally Stable, Porphyrinic Zr Metal−Organic Framework Exhibiting pH-Dependent Fluorescence. *J. Am. Chem. Soc.* **2013**, *135*, 13934−13938.
(14) Lan, G.; Li, Z.; Veroneau, S. S.; Zhu, Y.-Y.; Xu, Z.; Wang, C.; Lin, W. Photosensitizing Metal−Organic Layers for Efficient Sunlight-Driven Carbon Dioxide Reduction. *J. Am. Chem. Soc.* **2018**, *140*, 12369−12373.
(15) Rajasree, S. S.; Li, X.; Deria, P. Physical Properties of Porphyrin-Based Crystalline Metal−Organic Frameworks. *Commun. Chem.* **2021**, *4*, 47.
(16) Li, X.; Surendran Rajasree, S.; Yu, J.; Deria, P. The Role of Photoinduced Charge Transfer for Photocatalysis, Photoelectrocatalysis and Luminescence Sensing in Metal−Organic Frameworks. *Dalton Trans.* **2020**, *49*, 12892−12917.
(17) Deria, P.; Yu, J.; Smith, T.; Balaraman, R. P. Ground-State Versus Excited-State Interchromophoric Interaction: Topology Dependent Excimer Contribution in Metal−Organic Framework Photophysics. *J. Am. Chem. Soc.* **2017**, *139*, 5973−5983.
(18) Yu, J.; Anderson, R.; Li, X.; Xu, W.; Goswami, S.; Surendran Rajasree, S.; Maindan, K.; Gómez-Gualdrón, D. A.; Deria, P. Improving Energy Transfer within Metal−Organic Frameworks by Aligning Linker Transition Dipole Along Framework Axis. *J. Am. Chem. Soc.* **2020**, *142*, 11192−11202.
(19) Karagiaridi, O.; Bury, W.; Mondloch, J. E.; Hupp, J. T.; Farha, O. K. Solvent-Assisted Linker Exchange: An Alternative to the *De Novo* Synthesis of Unattainable Metal−Organic Frameworks. *Angew. Chem., Int. Ed.* **2014**, *53*, 4530−4540.
(20) Takaishi, S.; DeMarco, E. J.; Pellin, M. J.; Farha, O. K.; Hupp, J. T. Solvent-Assisted Linker Exchange (SALE) and Post-Assembly Metallation in Porphyrinic Metal−Organic Framework Materials. *Chem. Sci.* **2013**, *4*, 1509−1513.
(21) Goswami, S.; Yu, J.; Deria, P.; Hupp, J. T.; Patwardhan, S. Light Harvesting "Antenna" Behavior in Nu-1000. *ACS Energy Lett.* **2021**, *6*, 848−853.
(22) Van Wyk, A.; Smith, T.; Park, J.; Deria, P. Charge-Transfer within Zr-Based Metal−Organic Framework: The Role of Polar Node. *J. Am. Chem. Soc.* **2018**, *140*, 2756−2760.
(23) Williams, D. E.; Dolgopolova, E. A.; Godfrey, D. C.; Ermolaeva, E. D.; Pellechia, P. J.; Greytak, A. B.; Smith, M. D.; Avdoshenko, S. M.; Popov, A. A.; Shustova, N. B. Fulleretic Well-Defined Scaffolds: Donor−Fullerene Alignment through Metal Coordination and Its Effect on Photophysics. *Angew. Chem., Int. Ed.* **2016**, *55*, 9070−9074.
(24) Song, Y.; Li, Z.; Zhu, Y.; Feng, X.; Chen, J. S.; Kaufmann, M.; Wang, C.; Lin, W. Titanium Hydroxide Secondary Building Units in Metal−Organic Frameworks Catalyze Hydrogen Evolution under Visible Light. *J. Am. Chem. Soc.* **2019**, *141*, 12219−12223.
(25) Lin, S.; Cairnie, D. R.; Davis, D.; Chakraborty, A.; Cai, M.; Morris, A. J. Photoelectrochemical Alcohol Oxidation by Mixed-Linker Metal−Organic Frameworks. *Faraday Discuss.* **2021**, *225*, 371−383.
(26) Liu, X.; Kozlowska, M.; Okkali, T.; Wagner, D.; Higashino, T.; Brenner-Weiss, G.; Marschner, S. M.; Fu, Z.; Imahori, H.; Bräse, S.; Wenzel, W.; Wöll, C.; Heinke, L.; Zhang, Q. Photoconductivity in Metal−Organic Framework (Mof) Thin Films. *Angew. Chem., Int. Ed.* **2019**, *58*, 9590−9595.
(27) Dolgopolova, E. A.; Rice, A. M.; Smith, M. D.; Shustova, N. B. Photophysics, Dynamics, and Energy Transfer in Rigid Mimics of GFP-Based Systems. *Inorg. Chem.* **2016**, *55*, 7257−7264.
(28) Choi, S.; Jung, W.-J.; Park, K.; Kim, S.-Y.; Baeg, J.-O.; Kim, C. H.; Son, H.-J.; Pac, C.; Kang, S. O. Rapid Exciton Migration and Amplified Funneling Effects of Multi-Porphyrin Arrays in a Re(I)/Porphyrinic MOF Hybrid for Photocatalytic CO_2 Reduction. *ACS Appl. Mater. Interfaces* **2021**, *13*, 2710−2722.
(29) Lee, C. Y.; Farha, O. K.; Hong, B. J.; Sarjeant, A. A.; Nguyen, S. T.; Hupp, J. T. Light-Harvesting Metal−Organic Frameworks (MOFs): Efficient Strut-to-Strut Energy Transfer in Bodipy and Porphyrin-Based MOFs. *J. Am. Chem. Soc.* **2011**, *133*, 15858−15861.
(30) Dolgopolova, E. A.; Williams, D. E.; Greytak, A. B.; Rice, A. M.; Smith, M. D.; Krause, J. A.; Shustova, N. B. A Bio-Inspired Approach for Chromophore Communication: Ligand-to-Ligand and Host-to-Guest Energy Transfer in Hybrid Crystalline Scaffolds. *Angew. Chem., Int. Ed.* **2015**, *54*, 13639−13643.
(31) Fang, Z.-B.; Liu, T.-T.; Liu, J.; Jin, S.; Wu, X.-P.; Gong, X.-Q.; Wang, K.; Yin, Q.; Liu, T.-F.; Cao, R.; Zhou, H.-C. Boosting Interfacial Charge-Transfer Kinetics for Efficient Overall CO_2 Photoreduction via Rational Design of Coordination Spheres on Metal−Organic Frameworks. *J. Am. Chem. Soc.* **2020**, *142*, 12515−12523.
(32) Xia, Z.; He, C.; Wang, X.; Duan, C. Modifying Electron Transfer between Photoredox and Organocatalytic Units Via Framework Interpenetration for β-Carbonyl Functionalization. *Nat. Commun.* **2017**, *8*, 1−11.
(33) Yu, J.; Park, J.; Van Wyk, A.; Rumbles, G.; Deria, P. Excited-State Electronic Properties in Zr-Based Metal−Organic Frameworks as a Function of a Topological Network. *J. Am. Chem. Soc.* **2018**, *140*, 10488−10496.
(34) Goswami, S.; Yu, J.; Patwardhan, S.; Deria, P.; Hupp, J. T. Light-Harvesting "Antenna" Behavior in Nu-1000. *ACS Energy Lett.* **2021**, *6*, 848−853.

https://doi.org/10.1021/jacs.1c06629
J. Am. Chem. Soc. 2021, 143, 15286−15297

(35) Li, X.; Yu, J.; Gosztola, D. J.; Fry, H. C.; Deria, P. Wavelength-Dependent Energy and Charge Transfer in Mof: A Step toward Artificial Porous Light-Harvesting System. *J. Am. Chem. Soc.* **2019**, *141*, 16849−16857.
(36) Ramirez, C. E.; Chen, S.; Powers-Riggs, N. E.; Schlesinger, I.; Young, R. M.; Wasielewski, M. R. Symmetry-Breaking Charge Separation in the Solid State: Tetra(phenoxy)perylenediimide Polycrystalline Films. *J. Am. Chem. Soc.* **2020**, *142*, 18243−18250.
(37) Golden, J. H.; Estergreen, L.; Porter, T.; Tadle, A. C.; Sylvinson, M. R. D.; Facendola, J. W.; Kubiak, C. P.; Bradforth, S. E.; Thompson, M. E. Symmetry-Breaking Charge Transfer in Boron Dipyridylmethene (Dipyr) Dimers. *ACS Appl. Energy Mater.* **2018**, *1*, 1083−1095.
(38) Spenst, P.; Young, R. M.; Wasielewski, M. R.; Würthner, F. Guest and Solvent Modulated Photo-Driven Charge Separation and Triplet Generation in a Perylene Bisimide Cyclophane. *Chem. Sci.* **2016**, *7*, 5428−5434.
(39) Cook, R. E.; Phelan, B. T.; Kamire, R. J.; Majewski, M. B.; Young, R. M.; Wasielewski, M. R. Excimer Formation and Symmetry-Breaking Charge Transfer in Cofacial Perylene Dimers. *J. Phys. Chem. A* **2017**, *121*, 1607−1615.
(40) Giaimo, J. M.; Gusev, A. V.; Wasielewski, M. R. Excited-State Symmetry Breaking in Cofacial and Linear Dimers of a Green Perylenediimide Chlorophyll Analogue Leading to Ultrafast Charge Separation. *J. Am. Chem. Soc.* **2002**, *124*, 8530−8531.
(41) Wu, Y.; Young, R. M.; Frasconi, M.; Schneebeli, S. T.; Spenst, P.; Gardner, D. M.; Brown, K. E.; Würthner, F.; Stoddart, J. F.; Wasielewski, M. R. Ultrafast Photoinduced Symmetry-Breaking Charge Separation and Electron Sharing in Perylenediimide Molecular Triangles. *J. Am. Chem. Soc.* **2015**, *137*, 13236−13239.
(42) Webber, T. E.; Liu, W.-G.; Desai, S. P.; Lu, C. C.; Truhlar, D. G.; Penn, R. L. Role of a Modulator in the Synthesis of Phase-Pure Nu-1000. *ACS Appl. Mater. Interfaces* **2017**, *9*, 39342−39346.
(43) Lu, Z.; Liu, J.; Zhang, X.; Liao, Y.; Wang, R.; Zhang, K.; Lyu, J.; Farha, O. K.; Hupp, J. T. Node-Accessible Zirconium MOFs. *J. Am. Chem. Soc.* **2020**, *142*, 21110−21121.
(44) Snellenburg, J. J.; Laptenok, S.; Seger, R.; Mullen, K. M.; van Stokkum, I. H. M. Glotaran: A Java-Based Graphical User Interface for the R Package Timp. *J. Stat. Softw.* **2012**, *49*, 1−22.
(45) Formic acid is formed by the thermal decomposition of DMF in the presence of aqueous acid.
(46) Hod, I.; Farha, O. K.; Hupp, J. T. Modulating the Rate of Charge Transport in a Metal−Organic Framework Thin Film Using Host:Guest Chemistry. *Chem. Commun.* **2016**, *52*, 1705−1708.
(47) Celis-Salazar, P. J.; Cai, M.; Cucinell, C.; Ahrenholtz, S. R.; Epley, C. C.; Usov, P. M.; Morris, A. J. Independent Quantification of Electron and Ion Diffusion in Metal−Organic Frameworks Thin Films. *J. Am. Chem. Soc.* **2019**, *141*, 11947−11953.
(48) Liu, J.; Li, Z.; Zhang, X.; Otake, K.-i.; Zhang, L.; Peters, A. W.; Young, M. J.; Bedford, N. M.; Letourneau, S. P.; Mandia, D. J.; Elam, J. W.; Farha, O. K.; Hupp, J. T. Introducing Nonstructural Ligands to Zirconia-Like Metal−Organic Framework Nodes to Tune the Activity of Node-Supported Nickel Catalysts for Ethylene Hydrogenation. *ACS Catal.* **2019**, *9*, 3198−3207.
(49) Deria, P.; Mondloch, J. E.; Tylianakis, E.; Ghosh, P.; Bury, W.; Snurr, R. Q.; Hupp, J. T.; Farha, O. K. Perfluoroalkane Functionalization of Nu-1000 Via Solvent-Assisted Ligand Incorporation: Synthesis and CO_2 Adsorption Studies. *J. Am. Chem. Soc.* **2013**, *135*, 16801−16804.
(50) NU-1000, with 8-connected SBUs and four pairs of OH/OH_2 or its acidified variant with four pairs of $OH_2/OH_2(Cl)$, does not display the sharp 3780 cm^{-1} peak.
(51) A monodentate carboxylate binding, in place of one hydroxy ligand, would not provide the required locked SBUs and will leave more aqua ligands to display broad spectral feature at ca. 3657 cm^{-1} (or an enhanced red side shoulder of the 3675 cm^{-1} peak) and a new peak would appear at 3780 cm^{-1} upon heating by releasing the aqua ligand.
(52) Despite being an evenly distributed system, the β-connected porphyrin, loaded on average, one porphyrin per two nodes, is not symmetrically translated with respect to the crystal axes (Figure 2d).
(53) Liberman, I.; Shimoni, R.; Ifraemov, R.; Rozenberg, I.; Singh, C.; Hod, I. Active-Site Modulation in an Fe-Porphyrin-Based Metal−Organic Framework through Ligand Axial Coordination: Accelerating Electrocatalysis and Charge-Transport Kinetics. *J. Am. Chem. Soc.* **2020**, *142*, 1933−1940.
(54) Ray, D.; Goswami, S.; Duan, J.; Hupp, J. T.; Cramer, C. J.; Gagliardi, L. Tuning the Conductivity of Hexa-Zirconium(IV) Metal−Organic Frameworks by Encapsulating Heterofullerenes. *Chem. Mater.* **2021**, *33*, 1182−1189.
(55) Pratik, S. M.; Gagliardi, L.; Cramer, C. J. Boosting Photoelectric Conductivity in Porphyrin-Based MOFs Incorporating C60. *J. Phys. Chem. C* **2020**, *124*, 1878−1887.
(56) Kung, C.-W.; Otake, K.; Buru, C. T.; Goswami, S.; Cui, Y.; Hupp, J. T.; Spokoyny, A. M.; Farha, O. K. Increased Electrical Conductivity in a Mesoporous Metal−Organic Framework Featuring Metallacarboranes Guests. *J. Am. Chem. Soc.* **2018**, *140*, 3871−3875.
(57) Okinaga, K.; Suzuki, M. Synthesis of Nonplanar Meso-Trifluoromethyl-Substituted Tetrabenzoporphyrins Via Oxidation of Tetrabutanoporphyrins. *J. Porphyrins Phthalocyanines* **2020**, *24*, 135−142.
(58) Medforth, C. J.; Senge, M. O.; Smith, K. M.; Sparks, L. D.; Shelnutt, J. A. Nonplanar Distortion Modes for Highly Substituted Porphyrins. *J. Am. Chem. Soc.* **1992**, *114*, 9859−9869.
(59) Birks, J. B. Excimers. *Rep. Prog. Phys.* **1975**, *38*, 903−974.
(60) Because such complex formation is slower, at least slower than porphyrin $IC_{S2\rightarrow S1}$ ($\tau \lesssim 0.18$ ps), we can discard the possibility of [BFBP(Zn)S_2*−TBAPy] formation.
(61) While such features are difficult to probe, the spectral signature of a related species, [TFP(Zn)-TBAPy]*, may offer some clues (Figure 11); note that this is the excited species of a complex that formed at the ground state.
(62) Frischmann, P. D.; Mahata, K.; Würthner, F. Powering the Future of Molecular Artificial Photosynthesis with Light-Harvesting Metallosupramolecular Dye Assemblies. *Chem. Soc. Rev.* **2013**, *42*, 1847−1870.
(63) Heathcote, P.; Fyfe, P. K.; Jones, M. R. Reaction Centres: The Structure and Evolution of Biological Solar Power. *Trends Biochem. Sci.* **2002**, *27*, 79−87.

https://doi.org/10.1021/jacs.1c06629
J. Am. Chem. Soc. 2021, 143, 15286−15297